Electric Power Systems Research 214 (2023) 108826

Contents lists available at ScienceDirect

Electric Power Systems Research

journal homepage: www.elsevier.com/locate/epsr

Analysis of transient overvoltages and Self Protection Overvoltage of PV inverters through RT-CHIL

Prottay M. Adhikari [a,*], Luigi Vanfretti [a], Anja Banjac [b], Roland Bründlinger [b], Michael Ruppert [c], Michael Ropp [d]

[a] Department of Electrical, Computer and Systems Engineering, Rensselaer Polytechnic Institute, Troy, NY, United States of America
[b] Center for Energy, Austrian Institute of Technology, Austria
[c] JEM Engineering, Wappingers Falls, NY, United States of America
[d] Sandia National Labs, Albuquerque, NM, United States of America

ARTICLE INFO

Keywords:
Inverter protection
Self-Protection Overvoltage
Ground fault overvoltage
IEEE std 1547-2018
Real-time simulation
Controller-hardware-in-the-loop

ABSTRACT

In power systems, Single-Line-to-Ground (SLG) faults are the most common type of fault. When a three-phase four-wire system supplied by an ungrounded synchronous generator is subjected to SLG faults, the unfaulted phases are expected to exhibit significant ground-fault over-voltage (GFOV). Mitigation of this is via effective grounding, as described in IEEE Std 62.92.2. However, for inverter-based resources (IBRs), the physical mechanism that leads to GFOV in synchronous machines is not present. This paper investigates whether GFOV is a problem in IBRs, and whether conventional mitigation requirements, such as providing a grounding transformer (GTF), are suitable for IBR installations. To answer these questions, a Controller Hardware-in-the-Loop (CHIL) based performance analysis is conducted. To this end, different simulation models have been developed to analyze the IBRs control and protection response. The models are comprised of a 13.2 kV, 500 kW distribution system fed by a grid connected PV inverter which was simulated in Typhoon HIL 604 real time simulator, with a IEEE Std 1547-2018 compliant external physical controller connected in the loop. The experimental set-up and tests conducted are explained and results are analyzed, showing that effective grounding requirements are much different than those for traditional generators.

1. Introduction

This paper investigates the schemes for protecting PV inverters from transient overvoltages (TrOV) under single-line-to-ground (SLG) faults. To carry out this investigation, Typhoon HIL based real-time controller hardware in the loop (CHIL) models for a grid connected PV-inverter were developed. The paper is structured into five sections. The first section focuses on the motivation, presents a brief literature review, and enumerates the specific contributions of this article. The second section describes the experimental setup and methodologies in details. The third section presents the detailed simulation results, and the fourth section analyzes these results in the context of inverter protection. The final section concludes this article with additional discussions on the findings.

1.1. Motivation

It has been observed that up to 80% [1] of all the faults that occur in power systems, are single line to ground (SLG) faults. Theoretically, SLG faults occurring on a system supplied by ungrounded synchronous generators can lead to a Ground Fault Overvoltage (GFOV) of up to 173% of the nominal voltage on the unfaulted phases [2]. The theoretical derivation for this observation is carried out by the authors in [3]. To mitigate this over-voltage problem, the IEEE std C62.92.2 has proposed certain *effective grounding techniques* for synchronous generators. However, such existing methods require further validation and analysis in the context of their application in IBR based systems. To date, there is a gap in understanding on how IBR based systems would respond under SLG if existing *effective grounding techniques* are employed, and whether or not they are actually required for IBRs. Thus, the current work investigates the GFOV phenomenon and the application of existing mitigation techniques in the context of IBRs. Inverters, whether used for photovoltaic (PV) systems or energy storage facilities, typically include internal fast overvoltage protection mechanisms designed primarily to protect the inverter itself from damaging transients. These mechanisms, referred to as Self Protection Over-Voltage (SPOV) mechanisms, have the added benefit of causing the

* Corresponding author.
E-mail address: prottaymondaladhikari@gmail.com (P.M. Adhikari).

https://doi.org/10.1016/j.epsr.2022.108826
Received 11 August 2022; Received in revised form 9 September 2022; Accepted 19 September 2022
Available online 1 October 2022
0378-7796/© 2022 Elsevier B.V. All rights reserved.

Abbreviations

GFOV	Ground Fault Overvoltage
HIL	Hardware in the Loop
CHIL	Controller Hardware in the Loop
SLG	Single Line to Ground
IBR	Inverter Based Resources
GTF	Grounding Transformer
SPOV	Self Protection Overvoltage
LROV	Load Rejection Overvoltage
GLR	Generation to Load Ratio
SGC	Smart Grid Controller
MPPT	Maximum Power Point Tracking
RTS	Real-Time Simulator
GSU	Generator Step-Up
TrOV	Transient Overvoltage
ASGC	Austrian Institute of Technology Smart Grid Controller

inverter to cease to energize when the circuit voltage exceeds certain limits. The SPOV mechanisms thus can mitigate both ground-fault overvoltage (GFOV), and load-rejection overvoltage (LROV). With the SPOV function included in the inverter, the main purpose of this work is to demonstrate that overvoltages are mitigated with or without traditional *effective grounding techniques* employed in the system. To carry out this analysis, a controller-hardware-in-the-loop (CHIL) study is conducted by coupling a power system model designed specifically for this GFOV analysis to a *real-world* control/protection hardware device for IBRs. To this end, a model for a 13.2 kW, 500 kW distribution system including a grid connected PV unit was implemented in a real-time simulator (RTS). This choice was made because the response of IBRs is largely determined by the *real-world* software/hardware implementation of their control and protection features. The CHIL approach for testing control/protection equipment coupling an RTS with the actual control/protection hardware allows for a test-setup which reproduces highly transient power system behavior with full feedback between the control system and the plant-hardware. In RT-CHIL experiments, RTSs are used to simulate the response of a power system in real-time. In this work, the Typhoon HIL 604 RTS was used to model the grid connected PV system. To control the PV inverter, an IEEE Std 1547-2018-compliant control hardware, the *Austrian Institute of Technology Smart Grid Controller* (known as the ASGC or AIT SGC), was coupled with the RTS [4]. This configuration allows to evaluate how controller-hardware connected to the PV system would react to the SLG fault and to assess a possible GFOV. To modify the SPOV settings, the firmware on the controller was manipulated. This procedure is elaborated in Section 3.5.

1.2. Related works

The severity of GFOV observed in synchronous generators has been documented and theoretically analyzed previously [5]. This work showed that ungrounded 4 wire/3-phase distribution systems supplied by synchronous generators are susceptible to an over-voltage of up to 1.73 pu under SLG conditions, and evidence of this phenomena in various actual systems has been obtained through the survey presented by the authors in [6]. SLG faults are studied in great details for Romanian power grid in [7], and similar studies focusing on North America, have been published in [8]. Hence, there is a good understanding of GFOV due to faults for systems with conventional generators.

A recent study addressed the GFOV phenomena for IBR-based systems [3] and demonstrates that the resulting over-voltages in three-phase four-wire circuits serving Y-grounded impedance loads could be expected to reach no more than about 122% of the nominal voltage, which is below the requirements for effective grounding. However, they cannot be directly mitigated by the existing techniques in the IEEE Std 62.92.2 [9]. The results demonstrated by the authors in [10,11] established that if standard symmetrical-component analysis is used to solve for the impedance of a hypothetical grounding bank that would ensure that the voltages of both the unfaulted phases during an SLG fault would remain below the definition of "effectively grounded" above a certain GLR, it would yield a negative value. Thus there is no real-world solution for designing a GTF that would mitigate the overvoltages IBRs face under an SLG fault when they are operating under a high GLR (over 4.5). This phenomenon was explained by the fact that the negative-sequence voltage starts to dominate above that GLR.

This is because, typically grid-following IBRs cannot be modeled by ideal voltage sources. Instead, the responses of IBRs is largely defined by their fast-acting internal control and protection strategies [12], implemented in the firmware [13,14]. It is also important to note that the IBRs can exhibit both GFOV and Load Rejection Over-voltage (LROV), when subjected to an SLG condition as reported by the authors in [15]; and their Self-protection Overvoltage (SPOV) might interact with the GFOV or LROV phenomena. These hypotheses are addressed in this paper.

The use of digital real-time simulators is becoming increasingly relevant for technical performance analysis of energy resources and IBRs when integrated into the electrical grid. It is crucial to note that different existing RTS are widely disparate in terms of their modeling environments, component model libraries and the hardware they use. The surveys presented in [16,17] summarized intricate comparisons between these various real-time simulation platforms including but not limited to those from companies such as Opal-RT, Typhoon HIL, dSPACE, RTDS, etc. In this work, the discussion is constrained to the RTS from Typhoon HIL and related SW/HW infrastructure. The decision to use this simulation hardware was based on the compatibility of the ASGC control hardware with Typhoon HIL 604 RTS. Typhoon HIL supports SunSpec compliant inverter controller hardware, which needs to be connected to the real-time simulator that runs the inverter model via a breakout board. The ASGC is one of such controllers, while [4,18,19] have reported detailed descriptions of this hardware for different applications, such as the control the distributed energy sources (DER) being simulated on the real-time hardware.

1.3. Contributions

- This paper shows how appropriate SPOV settings are able to mitigate the TrOV and keep it from violating the constraints reported in IEEE std 1547-2018.
- This paper reports experimental results to demonstrate that traditional effective grounding techniques like grounding transformers are not suitable for mitigating TrOV for inverters under SLG, operating with higher GLRs (On predominantly Y-connected loads). Extensive sequence analyses were carried out to provide a theoretical justification of this phenomenon. The experimental observations were found to be corroborating to the research published in existing literature.

To achieve these two objectives, a Typhoon HIL based RT-CHIL test-setup was modeled and interfaced with an IEEE 1547 compliant controller hardware.

2. Experimental setup

2.1. Experiment's hardware infrastructure overview

The experiments conducted in this paper were carried out by simulating the power distribution circuit represented in Fig. 1 using

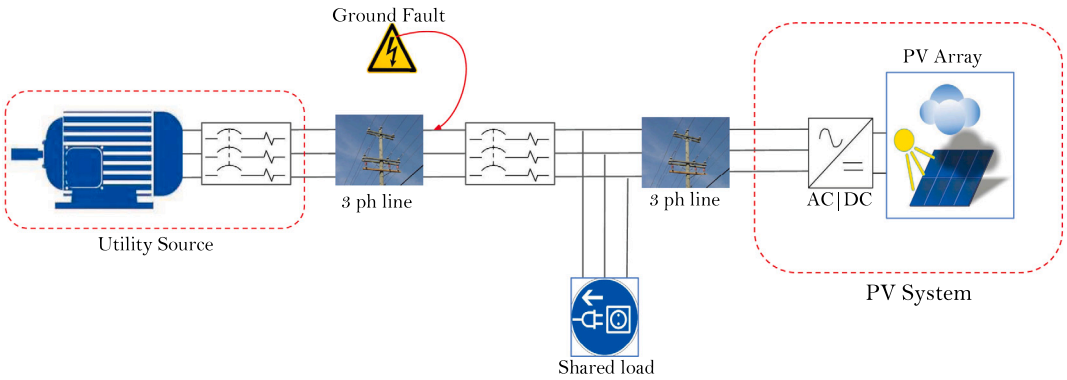

Fig. 1. Pictorial representation of the grid connected PV distribution feeder used in this work.

Table 1
Software used in the CHIL experiment.

Software type	Version	Function	Library/Selection
Firmware Manager	2020-release	Simulator Configuration	Control of Processor cores and Machine Cores, Memory Allocation
aBoot Flasher	3.1.1	Controller Configuration	Control of current & voltage configuration of the ASGC controller
Schematic Editor	2019/20	Designs the power circuit	Typhoon's proprietary library, User defined C functions, Initialization
HIL SCADA	8.4	Interact with the circuit running on simulator	HIL SCADA Widgets, Monitoring, Data Logging and Visual Library
	3.7	Interact with the controller hardware in loop	HIL SCADA Widgets, Monitoring, Data Logging and Visual Library

the Typhoon HIL-604 RTS. The inverter is controlled by the external controller-hardware (ASGC) generated PWM signals. Fig. 2.(b) shows a picture of the test bench with all these hardware components. Detailed description of these individual hardware components is presented in Appendix A.1.

2.2. Experiment's software overview

Table 1 summarizes the software tools utilized to carry out the GFOV experiment. It can be seen that most of these software tools are proprietary ones provided by Typhoon HIL and AIT. It needs to be noted that two different versions of the HIL SCADA software package are required. The latest version(8.4) interacts with the real-time simulator running the inverter model, and the older version (v3.7) interacts with the controller connected to the simulator. The functions of the different software are explained in detail in Appendix A.2.

Algorithm 1 Protocol for GFOV Experiments

```
/* SLG Fault Introduction                                   */
if ∠V_a − θ < ϵ then
    if Faulter=1 then
        BKR_F= CLOSE
        State= FLT
        EXIT to next function
    else
        BKR_F= OPEN
else
    Continue Simulation
/* Breaker Opening                                          */
while State=FLT do
    Wait (35 ms) ;
    do in parallel
        if ∠I_a < ϵ then
            BKR_A=OPEN
        if ∠I_b < ϵ then
            BKR_B=OPEN
        if ∠I_c < ϵ then
            BKR_C=OPEN
```

Table 2
Distribution system specifications.

Component	Specifications
Utility source	Line-to-line voltage, 13.2 kV 3 phase short circuit MVA, 180×10^6 X/R = 8 Line construction = 336AA (phase), 3/o (Neutral)
Distribution feeder	$Z_1 = 0.278 + j\ 0.682$ $Z_0 = 0.7575 + j1.9532$ Distance from PV to load, 3 miles Distance from load to breaker, 3 miles
DG transformer	3 phase, 480 V/13.2 kV kVA = 500, Z = 5%, X/R = 10 Configuration Yg-Yg
GTF (*if used*)	3 phase, 13.2 kV/13.2 kV kVA = 500, Z = 5%, X/R = 10 Configuration Yg-Δ
PV system	500 kW, 0 kVAR
Load	Constant power, Phase to ground kW = 500, kVAR = 0 Compensating capacitance: 29.5 kVAR *(at untuned condition)*

2.3. Experiment setup and protocol

This section describes how the aforementioned hardware/software were used to develop the experimental setup to analyze the GFOV phenomena.

Fig. 1 illustrates the model that was simulated on the Typhoon HIL 604. The specifications of the model's components are presented in Table 2. It needs to be noted that, the system shown in Fig. 1 also includes a capacitance-bank in parallel with the load. This capacitance-bank balances out the inductive reactive power consumed by the magnetization path of the 480 V/13200 V distribution transformer in order to help stabilize the frequency when the grid is disconnected.

To perform the GFOV experiments, the experimental protocol described in Algorithm 1 was followed. There are two interventions that need to be carefully applied, and to implement them one macro was written inside the Typhoon HIL SCADA (v8.4) tool.

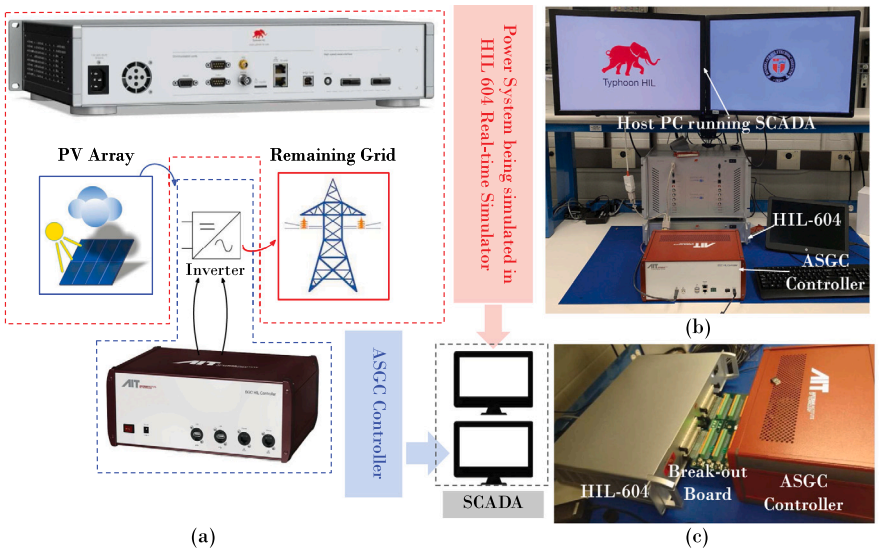

Fig. 2. (a) Pictorial representation of the experimental setup, (b) The physical experimental setup, (c) The interface between ASGC controller and Typhoon HIL 604.

First, the SLG fault is applied on the load bus. Next, the utility-side breaker waits 35 ms and then disconnects itself from the faulted portion of the system, leaving only the PV-inverter to feed the fault current. To ensure reproducibility in the experiments, the switch that applies the SLG was set to only operate when the voltage at phase A is at its highest (i.e. $\angle V_A = 90°(\theta)$). However, it was observed that, if this equality-relation ship is enforced, then the simulator often misses the 90° mark, because the PLL loop that computes the angle of the voltage signals had an update-rate of only 100us. Thus, an additional parameter ϵ was introduced, which is used to define a finite but small window during which the fault can strike. ϵ was set to 2.5°. This allowed to detect when the angle of the voltage waveform was within 2.5° of the 90° mark in order to apply the SLG. This sequence of events can also be visualized through Fig. 3.(a) and Algorithm 1.

Second, a similar approach was followed when disconnecting the grid from the remainder of the system. Upon waiting for 2 cycles (35 ms), the grid will be disconnected one phase at a time, only when the current on that phase is close to the zero-crossing. This was implemented by using the same parameter ϵ.

It is important to note that 35 ms is a very fast time for a standard distribution level breaker. However, in order to maximize the duration for which the inverter manages to provide the fault current (before disconnecting due to its own protection functionalities), the speed of the breaker was increased. The duration for which the inverter provides the fault current is the duration for which the GFOV may be observed. Consequently, all the analyses were performed on the measurements taken during this period. It needs to be noted that, the overall control strategy of the inverter is based on a standard constant P-Q algorithm. The inner current loops of this algorithm were used to control the d-axis and q-axis currents of the inverter.

3. Results and analysis

This section summarizes results from different analysis conducted.

3.1. Tuning of capacitor banks for GFOV sequence component analysis

The first set of results presented in this section is a CHIL simulation of the system with a Generation to Load Ratio (GLR) of 1.0. These simulation results are summarized in Fig. 3(a)–(d). To emphasize the utility of a well-tuned capacitor bank, Fig. 3(b) is reproduced in Fig. 4(a). It can be seen from Fig. 4(a), that after the utility detects the SLG fault and disconnects itself, the inverter only manages to sustain itself for 3 cycles. During these 3 cycles, there was a maximum of 7.8% over-voltage observed on the unfaulted phases. In Fig. 4(b), the employment of a capacitor bank increases the number of cycles (> 10 cycles) the inverter manages to sustain itself after the injection of the fault.

It can be seen upon careful observation of the waveforms in Fig. 4 (a)–(b) for $0.55\ \text{s} \leq t \leq 0.6\ \text{s}$, that the magnitude of over-voltage is much lower than what was observed (73%) in synchronous generators, irrespective of whether a capacitor bank is used.

It was also observed that (without capacitance bank) during these 3 post-fault cycles, the frequency varies rapidly (red plot in Fig. 4(c)), and the inverter ultimately disconnects due to the operation of over-frequency relay. Because, the frequency was not constant, the relative phase angles were varying, and thus, it is theoretically difficult to apply symmetrical components to this situation (i.e. Fig. 4(a)). However, in order to evaluate the protection schemes for such systems under SLG faults, and better understand how the measurement and control system of the inverter respond to such conditions, it is useful to perform the symmetrical component analysis. To apply the symmetrical component analysis frequency needs to be relatively constant. To achieve this, a *tuned* capacitance bank was connected in parallel with the resistive load. Tuning of capacitance-banks is a well-researched topic which has been addressed in [20]. For this particular research, the sizing of the capacitance bank (< 10% of the system capacity) was decided based on the ratios reported by the authors in [21]. The tuned capacitance bank had a capacitance of 1.75 uF per phase. Upon successful tuning, the inverter manages to operate at a reasonably fixed frequency for a few cycles (blue plot in Fig. 4(c)) even after the utility has been disconnected. It must be noted that regardless of having tuned the capacitance-bank for analysis purposes, the inverter will disconnect itself after a few additional cycles of islanded operation as shown by other experimental studies [22]. In order to investigate the nature and source of the overvoltage, a detailed symmetrical component analysis was performed on this modified model with tuned capacitance banks, during those cycles. The three-phase voltage-responses of the system with and without tuned capacitors are shown in Fig. 4. It can be seen that the inverter can operate for a much longer duration when the capacitor banks are carefully tuned. Fig. 4.(c) shows that the frequency estimated by the PLL loop goes beyond the permissible limit within 2–3 cycles if the capacitance banks are not tuned properly. Under the new conditions the sequence diagram under faulted condition can be determined. When the utility has already disconnected itself from the inverter and the load, the sequence diagram is shown in Fig. 5(a).

Fig. 6(a)–(b) exhibit the phase currents from the inverter's side, and the phase currents measured on the load. Fig. 6(c)–(d) illustrate

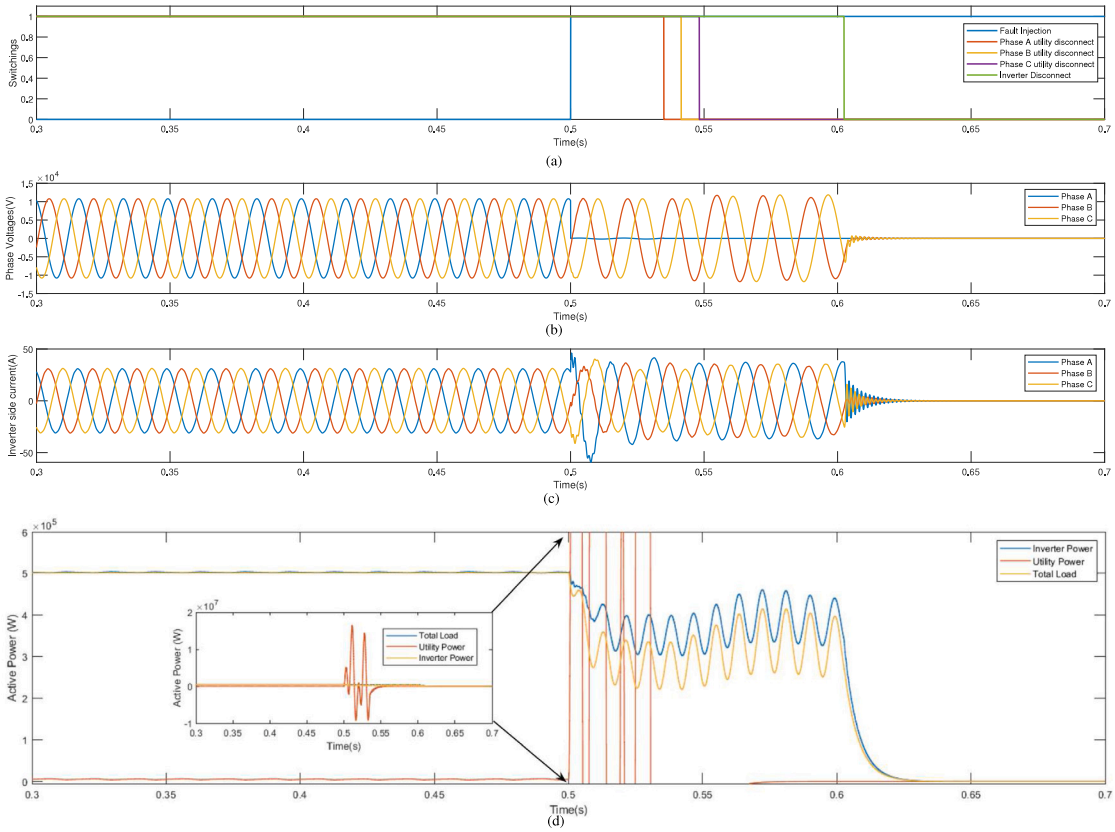

Fig. 3. CHIL simulation under GLR 1.0: (a) operation of the breakers, (b) phase voltages, (c) phase currents (PV-Inverter), (d) active power provided by the utility and the PV source.

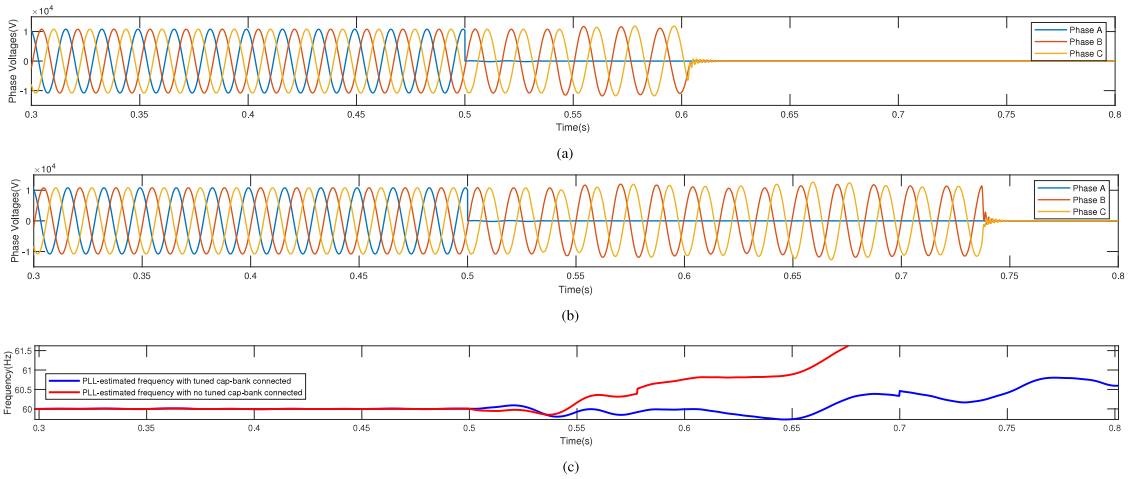

Fig. 4. Effect of capacitance-tuning: (a) phase voltages under slg without tuned capacitor bank, (b) phase voltages under SLG with tuned capacitor bank, (c) frequency estimation by the measurement system under SLG.

the symmetrical components of the currents plotted in Fig. 6(a)–(b) respectively. Notably, for the current from the PV-inverter side, the zero-sequence current was negligible while the negative-sequence current was non-negligible (e.g. around the 0.65 s mark, the zero sequence current is close to zero, while the negative sequence current is close to $1.5A$). For the currents observed from the load, both the negative-sequence and zero-sequence currents are significant. This is expected because the phase-A current is zero while the phase-B and phase-C currents are higher than their unfaulted values.

To establish how these results relate to the circuit of Fig. 5(a), instantaneous values observed at $t = 0.6$ s seconds were considered. Applying KCL in the circuit of Fig. 5(a) gives:

$$I_0 = I_{PV(+)} - I_{load(+)} \tag{1a}$$

$$I_0 = I_{PV(-)} - I_{load(-)}. \tag{1b}$$

Next, applying KVL on Fig. 5(a) yields:

$$V_+ = I_{load(+)} \times Z_{ph}, \tag{2a}$$

$$V_- = I_{load(-)} \times Z_{ph} \tag{2b}$$

$$V_0 = I_{load(0)} \times Z_{ph}. \tag{2c}$$

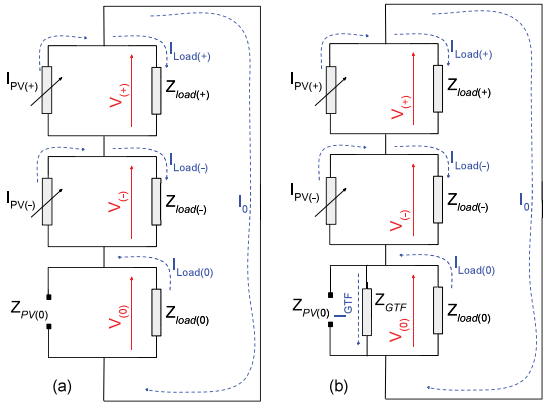

Fig. 5. Sequence diagram under SLG: (a) Without the GTF, (b) With the GTF.

Table 3
Sequence components of Fig. 5(a) at t = 0.65 s.

Eqn	Numerical validation	
KCL(1)	$I_{PV(-)} - I_{load(-)}$	$= 1.93\angle -17.6° - 7.34\angle -178° = 9.18\angle -3.1°$
	$I_{PV(+)} - I_{load(+)}$	$= 26.07\angle 0° - 16.9\angle 1.7° = 9.175\angle -2°$
	$I_{load(0)} = I_0$	$= -9.18\angle 178° = 9.18\angle -2°$
KVL(2)	$V_- = Z_{ph} \times I_{load(-)}$	$= 339\angle -12.1° \times 7.34\angle -178° = 2488.26\angle -190.1°$
	$V_+ = Z_{ph} \times I_{load(+)}$	$= 339\angle -12.1° \times 16.9\angle 1.7° = 5729.1\angle -10.4°$
	$V_0 = Z_{ph} \times I_{load(0)}$	$= 339\angle -12.1° \times 9.18\angle -182° = 3112.02\angle -194.1°$
(3)	$V_b = a^2V_+ + aV_- + V_0$	$= 8361\angle -134.4° = 1.096$ pu
	$V_c = aV_+ + a^2V_- + V_0$	$= 8273\angle 112.8° = 1.085$ pu

The values of the phase currents for the PV inverter and the load at t = 0.65 were logged from the observation made in Fig. 6. These values are verified by using (1) and (2). The results are summarized in the first two rows of Table 3. Having calculated the voltage-sequence components, those values were used to verify the phase voltages using:

$$V_b = a^2V_+ + aV_- + V_0 \tag{3a}$$

$$V_c = aV_+ + a^2V_- + V_0. \tag{3b}$$

The results for the unfaulted phases B and C are summarized in the third row of Table 3. It can be seen that there are some minor over-voltages in the unfaulted phases. This is consistent with the observations made in Fig. 6(b).

3.2. GFOV and GLR

The next set of experiment was to vary the GLR and study the effect of GLR on GFOV. This was achieved by varying the load while keeping the generation from the PV-inverter constant. This type of study is reported in IEEE Std 62.92.6.-2017. In this work, the trend of GFOV with varying GLR was compared with those reported in the IEEE Std. This comparison is shown in Fig. 7. It is also observed that overvoltage for IBRs is a bigger problem for larger values of GLR than it is for smaller values of GLR. It is also illustrated that at a GLR of 1.0, the GFOV is not as severe as it is for synchronous generators.

3.3. Impact of conventional GFOV mitigation

The next step in this experimentation was the application of traditional over-voltage mitigation techniques in this system. While methods like injection of neutral bus and using ground fault neutralizers are sporadically used in improving the grounding efficiency of power systems, most industries utilize grounding transformers for effective grounding and lowering the coefficient of grounding. For this particular work, a grounding transformer was incorporated within the circuit (and the capacitance bank had to be re-tuned to obtain well-sustained results). Two different types of connections are used in grounding transformers (GTF): (a) ZigZag or (b) Yg- Δ. Because the ZigZag transformer was not available in the model library, the Yg- Δ connection for the GTF was used. The GTF size was varied from 100 kVA to. 500 kVA. The maximum overvoltages at varying size of the GTF is plotted in Fig. 8. It can be seen in Fig. 8 that, the reduction of maximum overvoltage increases with the increasing size of the GTF, although the magnitude of reduction is minimal. The sequence analysis reported in this paper were performed using the 500 kVA GTF. It is to be noted that this size of GTF is a large one (at 500 kVA, the GTF is of the same rating as the distribution transformer), which was chosen to emphasize its impacts on the circuit. Under an SLG fault, the sequence diagram is also modified to include the GTF. This modified sequence diagram is illustrated in Fig. 5(b). The modified system model was simulated for a GLR of 1.0. The KCL applied to this sequence diagram yields:

$$I_0 - I_{GTF} = I_{PV(+)} - I_{load(+)} \tag{4a}$$

$$I_0 - I_{GTF} = I_{PV(-)} - I_{load(-)} \tag{4b}$$

Table 4
Sequence components of Fig. 5(b) at t = 0.65 s.

Eqn	Numerical validation	
(4)	$I_{PV(-)} - I_{load(-)}$	$= 2.99\angle 106° - 11.8\angle 199° = 12.31\angle 33.2°$
	$I_{PV(+)} - I_{load(+)}$	$= 25.9\angle 26.1° - 14.02\angle 15.6° = 12.37\angle 37°$
	$I_{load(0)} - I_{GTF} = I_0$	$= -10.25\angle 29° + 2.35\angle -142° = -12.37\angle 31°$
(2)	$V_- = Z_{ph} \times I_{load(-)}$	$= 331.1\angle -18.1° \times 11.8\angle 199° = 3906\angle 180.9°$
	$V_+ = Z_{ph} \times I_{load(+)}$	$= 331.1\angle -18.1° \times 14.02\angle 15.6° = 4642\angle -2.5°$
	$V_0 = Z_{ph} \times I_{load(0)}$	$= 331.1\angle -18.1° \times 2.35\angle -142° = 778.1\angle -160.1°$
(3)	$V_b = a^2V_+ + aV_- + V_0$	$= 7841\angle -99.8° = 1.03$ pu
	$V_c = aV_+ + a^2V_- + V_0$	$= 7151\angle 97.31° = 0.93$ pu

Eqs. (4) and (2) were used to verify the experiment results for the modified system with GTF in Table 4. It can be seen that the zero-sequence voltage is significantly reduced by the addition of the grounding transformer, but this reduction in zero-sequence voltage was not reflected in the negative sequence circuit. In fact, there was a minor increase in the negative sequence voltage upon the introduction of the GTF.

Hence, the improvement in TrOV by incorporating GTFs is negligible. It can also be seen that one of the unfaulted phases bears a lower voltage than the other. This is consistent with the observation in Fig. 9(b), and those reported in [10]. It is also to be noted, that the GTF provides a significant amount of zero sequence current into the network as shown in Fig. 10(e). This influx of zero sequence current changes the behavior of the circuit significantly, but it does not improve the existing overvoltage (around 10%) in the system. The phasor diagrams corresponding to the observations noted in Tables 3 and 4 are shown in Fig. 13.

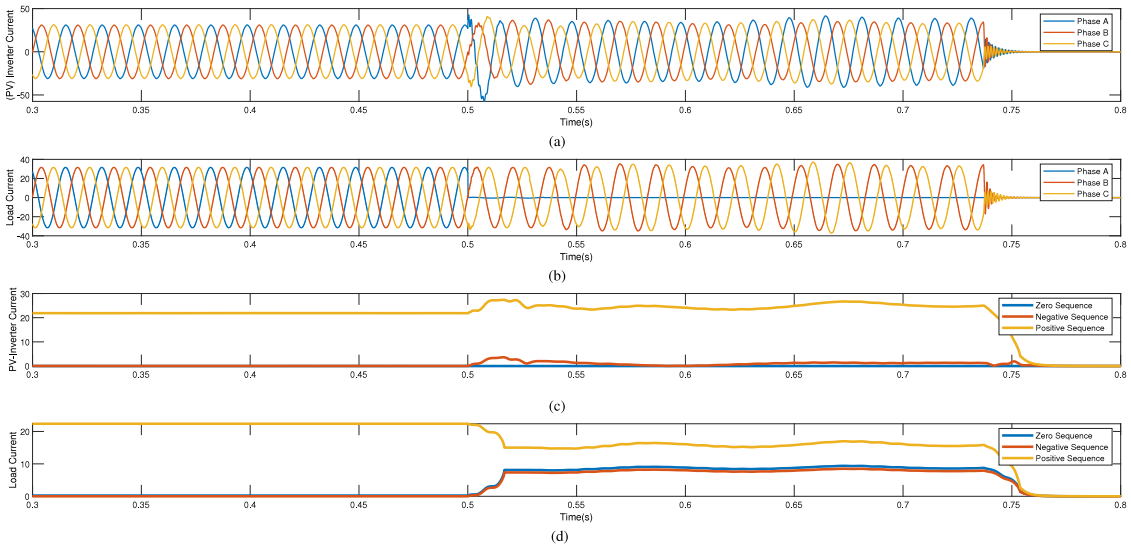

Fig. 6. Current measurements when there is no GTF in the circuit: (a) 3-phase currents from PV inverter, (b) 3-phase load current, (c) Sequence components of currents from PV inverter, (d) Sequence components of load current.

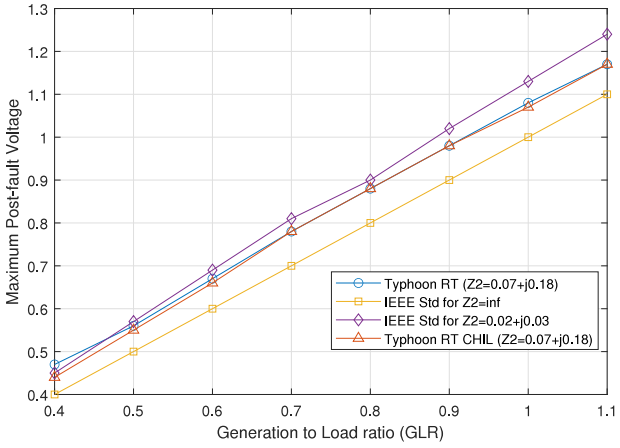

Fig. 7. Variation of overvoltage with increasing GLR.

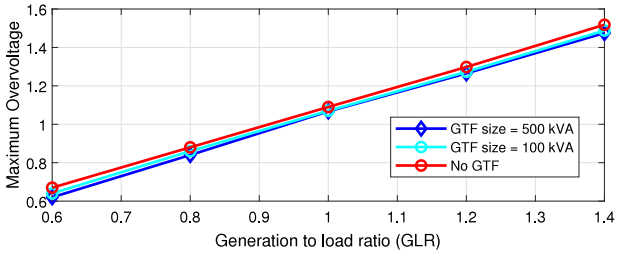

Fig. 8. Variation of overvoltage with varying size of GTF.

3.4. Impact of the power-factor in the load

In this experiment the configuration of the existing load was modified to include inductive components within it (The capacitance bank was re-tuned to achieve well-sustained results). The resultant power factor after this modification was set to be 0.9 (lag). Fig. 14(a) shows the GFOV while the load pf is 0.9 and the active power is set to 500 kW, resulting in an apparent power of 556 kVA. The observed maximum overvoltage in this experiment was close to 9%. Similarly, Fig. 14(b) demonstrates the overvoltages when the load pf is 0.9 and the apparent power is 463 kVA. This yields an active power output of 416.6 kW, and a GLR of 1.2 if the inverter output is kept constant at 500 kW. The observed maximum overvoltage in these experiment was close to 29%. These results are consistent with the results obtained with upf loads at GLR = 1.0 and 1.2, which are presented in the second column of Table 5. Thus, it can be concluded that, the inductive reactive power component of the load does **not** effect the maximum GFOV as long as the active power is maintained constant.

3.5. Impact of SPOV

It needs to be kept in mind that most modern inverters have a Self-Protection Over-voltage (SPOV) function that rapidly stops switch gating in case of an over-voltage. This operation is extremely fast and and is commonly based on instantaneous values of the voltages. This SPOV mechanism is very helpful in mitigating TrOV while the IBR operates at a GLR significantly over 1.0. Many inverters have the SPOV setting fixed at 1.3 pu or 1.4 pu, i.e. the inverter will disconnect in few hundred microseconds if it detects an over-voltage over 30% or 40%, respectively. The ASGC has a default SPOV setting **fixed at 1.3**. Because the TrOV varies almost linearly with the GLR, the SPOV for the inverter was automatically triggered whenever simulations were run for GLRs over 1.3. This makes experimenting with higher GLRs impossible without making modifications to the hardware. It also demonstrated that the internal SPOV settings of the ASGC controller hardware was very effective in mitigating the TrOV.

In order to run experiments with higher GLRs, the controller firmware was modified. However, direct modification of the SPOV is not possible, i.e. it is not possible to change the value from 1.3 to a higher value directly. Instead, it was necessary to change the *nominal voltage* parameter from 480 V to 600 V. This makes the new set-point for SPOV trigger at $600 \times 1.3 = 780$ V, which is 1.625 times of the previous nominal voltage of 480 V. Thus, under this new firmware settings, it is possible to run experiments which might result in higher over-voltages up to 1.625 pu. In Table 5, the results presented in blue colored rows are obtained from experiments performed with this new controller-firmware.

For the purpose of simplicity, this paper refers to the SPOV value of 1.3 as SPOV `enabled`, and the SPOV value of 1.625 as SPOV effectively `disabled`.

For a GLR of 1.3, two experiments were performed with the SPOV settings `disabled` and `enabled` respectively, in order to show how the SPOV interacts with the GFOV experiments. While the SPOV setting

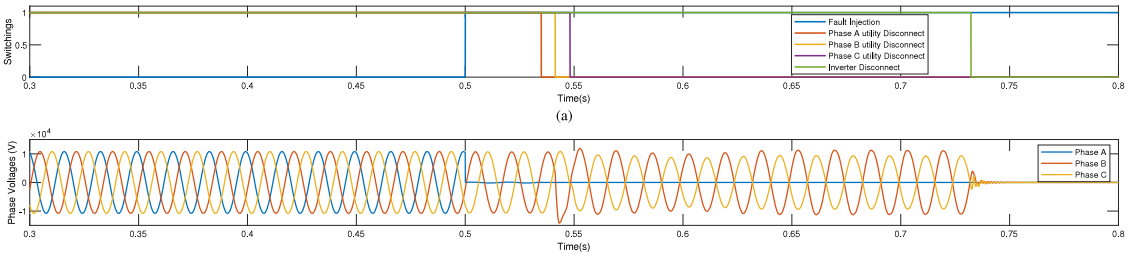

Fig. 9. Overvoltage simulation with GLR = 1.0 and GTF: (a) Switching sequence, (b) Phase voltages.

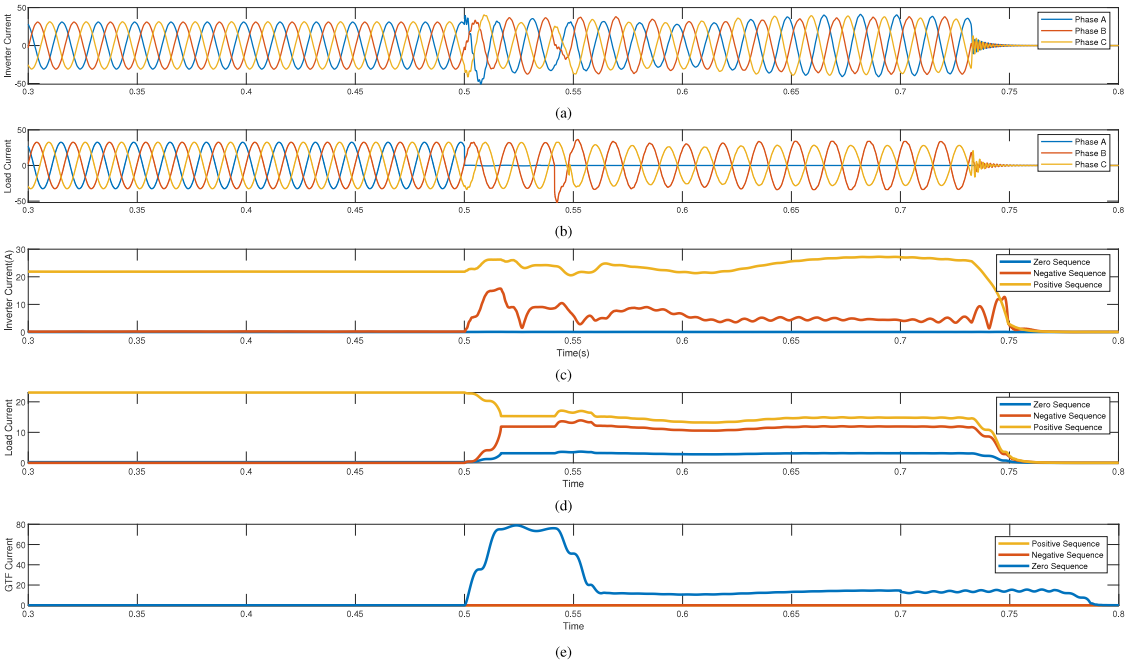

Fig. 10. Currents with GTF in the circuit: (a) 3-phase currents from PV inverter, (b) 3-phase load current, (c) Sequence components of PV inverter currents (d) Sequence components of load current (e) Sequence components of the GTF currents.

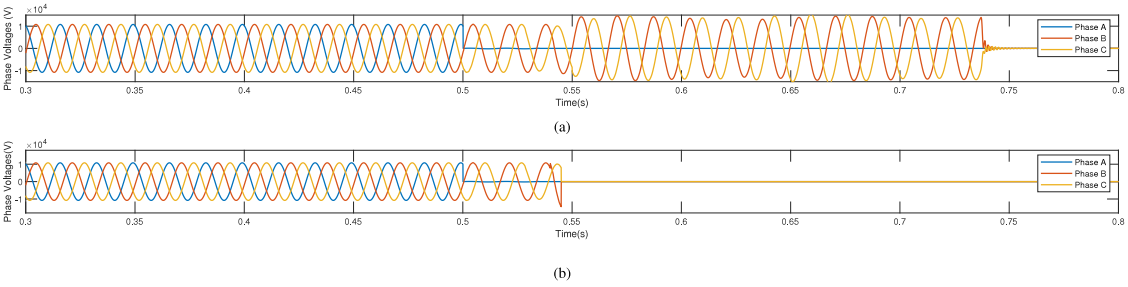

Fig. 11. SPOV interaction with the TrOV simulations for GLR=1.30: (a) When SPOV is disabled at 1.3 (b) When SPOV is enabled at 1.3.

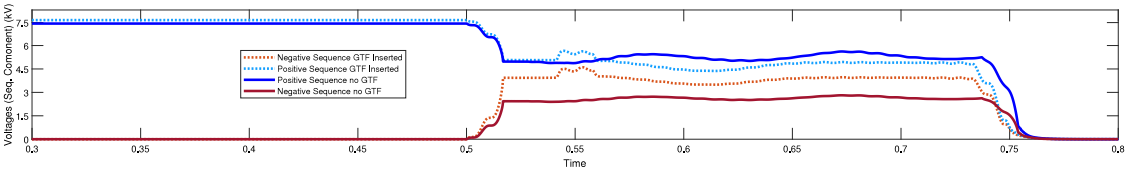

Fig. 12. Comparison of sequence components of the voltages with and without the grounding transformer.

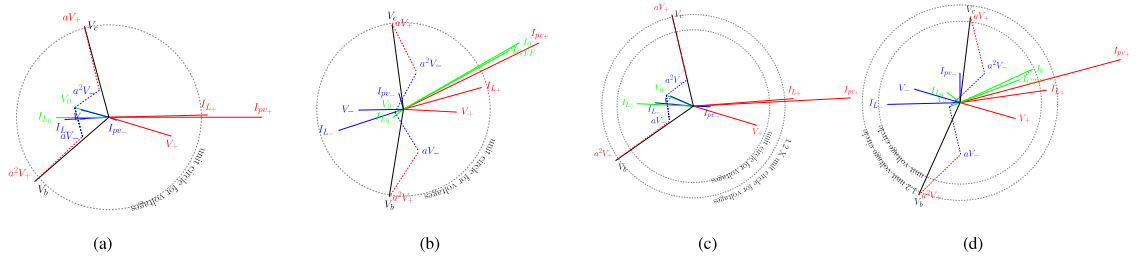

(a) (b) (c) (d)

Fig. 13. Phasor Diagrams: (a) No GTF inserted, GLR = 1, (b) GTF inserted, GLR = 1, (c) No GTF inserted, GLR = 1.2, (d) GTF inserted, GLR = 1.2. (Red=Positive Sequence, Blue=Negative Sequence, Green=Zero Sequence, Black= Phase Voltages).

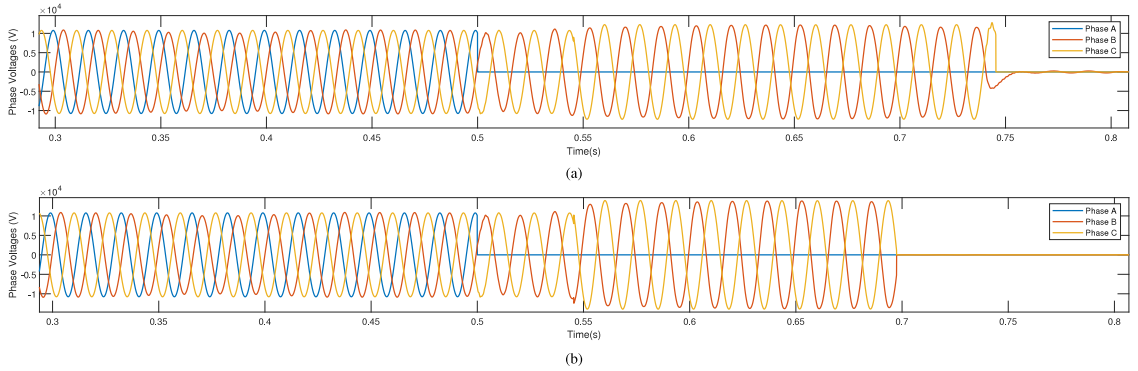

(a)

(b)

Fig. 14. TrOV experimentation with non-UPF (0.9 lag) loads: (a) While GLR = 1.0, (b) While GLR = 1.2.

Table 5
TrOV variation with and without GTF.

GLR	Max TrOV without GTF	Max TrOV with GTF
0.6	0.67	0.62
0.7	0.78	0.73
0.8	0.88	0.84
0.9	0.99	0.935
1	1.09	1.067
1.1	1.178	1.15
1.2	1.298	1.265
1.3	1.412	1.384
1.4	1.518	1.475
1.5	1.60	1.559
1.6	Unsustained	Unsustained

is kept as `disabled`, the overvoltage simulations were run and the results are archived in Fig. 11(a). It was observed that the overvoltage was close to 40% and the system experienced this level of overvoltage for over 10 cycles. However, when the firmware is changed to the version with lower voltage rating, i.e. SPOV `enabled`, the system disconnects instantaneously after it experience the 30% overvoltage the first time. This response is shown in Fig. 11(b). The SPOV operation can also be confirmed by investigating the flags `Protection.OC` and `Vbn.max` of the controller hardware, both of which were observed to be changed to 1, after running this test with SPOV `enabled`.

4. Summary and analysis of experimental results

4.1. Impact of TrOV in IBRs

The experimental results summarized in Section 3 establishes that inverter based DER systems are less prone to TrOV compared to synchronous generators. However, for systems with higher GLR, the overvoltage (more specifically, LROV) can still be significant. The overvoltage effect would also be prominent for IBRs supplying loads of lower power factors.

Crucially, it was observed that conventional grounding transformers can **not** mitigate these overvoltages properly. This is because, the introduction of GTFs increase the negative sequence voltage slightly, in spite of reducing the zero sequence voltage by manipulating the zero sequence impedance. This is illustrated in Figs. 12 and 13. Additionally, with the rising GLR, there is significant increase in TrOV is due to the LROV phenomenon (which originates from the positive sequence circuit). To construct the phasor diagrams presented in Fig. 13, the instantaneous values of currents and voltages at t=0.625s were used.

4.2. Importance of SPOV settings in IBRs

Building upon the previous observation, it can be stated that an inverter operating under a high GLR, remains vulnerable to TrOV (due to LROV and GFOV) under SLG conditions even if a grounding transformer is utilized in the system to mitigate overvoltages. However, based on the results shown in Fig. 11(a)–(b) it can be hypothesized that the IEEE 1547-2018 recommended SPOV settings are extremely useful in protecting inverter based DERs from such TrOV. Table 6 illustrates the effectiveness of appropriate SPOV settings to mitigate overvoltages in IBRs. It demonstrates the effect of setting a lower (i.e. 1.3) value of SPOV while the IBRs are providing (i) a load with 50% share of Yg load and (ii) a load with 100% share of Yg load. In this table, the observations in 'red' exceed the acceptable limit of maximum overvoltage according to the IEEE 1547-2018 std. These overvoltages were mitigated by simply setting a more restrictive SPOV value of 1.3.

Apart from the maximum overvoltage constraints, IEEE std 1547-2018 also proposes predetermined upper-limits for the *cumulative overvoltage durations* for certain discrete overvoltage levels (from 1.3 pu to 2 pu). Fig. 15 demonstrates that without the SPOV settings enabled, the cumulative overvoltage-duration for the observed voltages fall outside the acceptable operating region when the system is subjected to SLG. The estimation for cumulative overvoltage duration can be carried out by using the relationship $T_{cumulative_{1.3}} = N_{cycles} \times T_{1.3}$ where N_{cycles} is the number of cycles the inverter can sustain itself post-breaker operation, and $T_{1.3}$ is the amount of time in each cycle during which the instantaneous voltage of the unfaulted phase is over 1.3 pu. It is

Table 6
Impact of (i) SPOV settings and (ii) Percentage of Y-connected loads- on the maximum overvoltage.

GLR	Overvoltage with 100% Yg load		Overvoltage with 50% Yg load	
	SPOV = 1.3	SPOV = 1.625	SPOV = 1.3	SPOV = 1.625
0.6	0.67	0.67	0.96	0.96
0.7	0.78	0.78	1.14	1.15
0.8	0.88	0.88	1.23	1.23
0.9	0.99	0.99	Unsustained	1.28
1.0	1.09	1.09	Unsustained	1.32
1.1	1.2	1.18	Unsustained	1.49
1.2	1.3	1.3	Unsustained	Unsustained
1.3	Unsustained	1.412	Unsustained	Unsustained
1.4	Unsustained	1.518	Unsustained	Unsustained
1.5	Unsustained	1.6	Unsustained	Unsustained
1.6	Unsustained	Unsustained	Unsustained	Unsustained

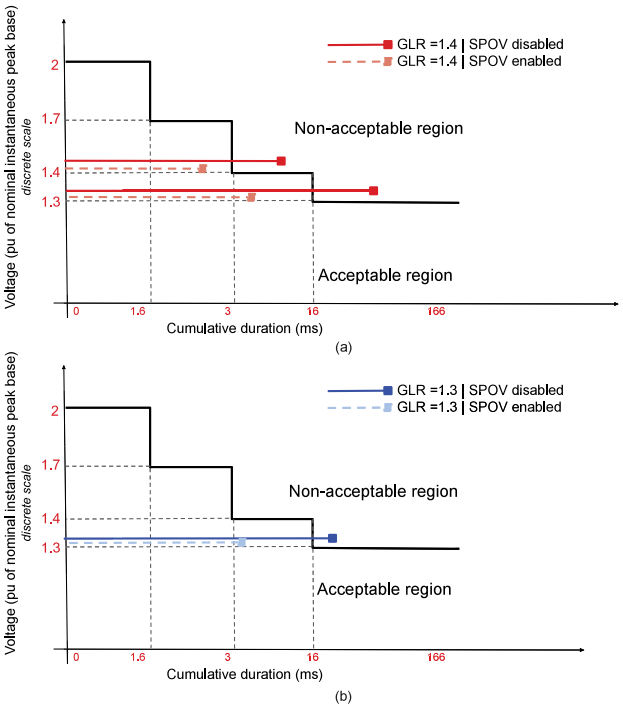

Fig. 15. Cumulative overvoltage duration calculation (a) GLR = 1.3 (b) GLR = 1.4.

to be noted that, for experiments where the maximum overvoltage is over 1.4 pu, both $T_{cumulative_{1.3}}$ and $T_{cumulative_{1.4}}$ need to be computed. Similarly, for experiments where the maximum voltage was over 1.5 pu, three cumulative times $T_{cumulative_{1.3}}$, $T_{cumulative_{1.4}}$ and $T_{cumulative_{1.5}}$ need to be calculated. The observations presented in Fig. 15 establishes that a restrictive SPOV setting is crucial to protect IBRs from *cumulative overvoltage duration* violations.

5. Conclusions and future works

Real-time CHIL simulation facilitates understanding of how modern inverter controls interact with conventional power grids without the need of traditional modeling assumptions used in traditional off-line studies or to perform field experiments. This paper presented CHIL simulation results for SLG faults in a distribution network with grid connected PV-inverters, and demonstrated that the GFOV in such systems is much less severe than they are when conventional synchronous generators are used. It was also demonstrated that overvoltage becomes more severe at higher generation to load (GLR) ratios. A standard GFOV mitigation technique, i.e. grounding transformers (GTF), was applied to the system and only a marginal improvement was observed in terms of overvoltage reduction. Detailed sequence component analysis was performed and it was observed that the resulting over-voltage observed was generated predominantly from the negative sequence network. Since, GTFs change the zero sequence network, they were unable to completely mitigate the over-voltages. However, since the magnitude of the over-voltage was small for standard operating conditions, the grounding needs are much lower than those of synchronous generators. Finally, the effectiveness of the controller's SPOV was analyzed, showing that this mechanism will disconnect the inverter when an over-voltage occurs.

The most important conclusion of this research is that, grounding transformers can **not** prevent transient overvoltages for IBRs under SLG fault. Utilities are still reluctant to abandon this practice due to a lack of sufficiently-convincing information, which the authors believe is leading to increased capital expenditures in the interconnection of new inverter-based plants. The analysis identified how a supplemental ground source e.g. GTF, will not completely eliminate a GFOV condition as they can only reduce the zero sequence impedance of the system. In systems with higher GLRs, both the zero sequence and the negative sequence network contributes to the overvoltages on the unfaulted phases. The contribution from the negative sequence circuit is not compensated by the GTF, and thus it dominates the overvoltage phenomenon, especially at the higher GLRs. Grounding transformers can also lead to negative impacts on distribution circuits, such as desensitizing the utility ground relaying, increased arc flash energy and blinding of the DERs to single phase open circuits. In addition, without the supplemental ground source (i.e. the GTF) on the utility system, the negative impacts will not be present which include issues with single phase open detection and the desensitization of utility ground relaying. Thus, there are tangible positive consequences of not using the GTFs within the network.

The results of this paper support the hypothesis that the **SPOV function will mitigate excessive overvoltages** during a ground fault on a distribution circuit when installed with a wye-ground/wye-ground interconnection transformer. The same function will also mitigate load rejection overvoltages (LROV).

The experiments reported in this paper were performed only in a controller-hardware-in-the-loop (CHIL) configuration. Thus, it is advisable to perform similar experiments in **power**-hardware-in-the-loop setting with industry-grade inverters before proposing actual modifications to the IEEE standards. These experiments would require a safe laboratory space and personnel experienced in operating such high-voltage equipments. It is important to take into account that, the current paper only analyzes experimental results featuring IBRs feeding Y-connected loads. In reality, Δ configurations are occasionally used in distribution level networks. Hence, it is important to validate the protective features of inverters for such connections. These experiments were beyond the scope of the current paper, and they require further exploration.

CRediT authorship contribution statement

Prottay M. Adhikari: Conceptualization, Methodology, Data curation, Investigation, Visualisation, Writing – original draft. **Luigi Vanfretti:** Conceptualization, Writing – review & editing, Supervision. **Anja Banjac:** Software, Methodology. **Roland Bründlinger:** Software, Methodology. **Michael Ruppert:** Conceptualization, Funding, Supervision. **Michael Ropp:** Conceptualization, Funding, Supervision.

Declaration of competing interest

The authors declare the following financial interests/personal relationships which may be considered as potential competing interests: Prottay M. Adhikari reports financial support was provided by New York State Energy Research Development Authority.

Data availability

No data was used for the research described in the article.

Acknowledgments

The authors wish to thank Austrian Institute of Technology for their contributions to this project.

This work was supported in part by the New York State Energy Research and Development Authority (NYSERDA) under agreements 137948 and 149165. NYSERDA has not reviewed the information contained herein and the opinions expressed in this paper do not necessarily reflect those of NYSERDA or of the state of New York.

Appendix. The hardware and software utilized for the experiments

A.1. Hardware utilization in details

The hardware components used for experimentation are described in this section.

A.1.1. HIL-604 real-time simulator

HIL-604 is an RTS manufactured by Typhoon HIL. It is predominantly used to simulate power-electronic systems and microgrids in real-time for different applications, including CHIL. The computational hardware of the HIL-604 consists of Xilinx Vertex FPGA cores alongside ARM real-time processors. The RTS has both digital and analog input and output channels that can be used to interface it with an external hardware. The simulator has been tested by the manufacturer for accuracy for a simulation speed up to 2 MHz, while the PWM functionalities operate satisfactorily down to a resolution of 20 ns. The simulator is controlled by the user through the *Typhoon HIL SCADA* or *HIL Schematic Editor* software that run in a separate PC and communicate with the RTS via a USB 2.0 interface. While, this paper focuses on external hardware based control of the real-time model of the inverter, it is possible to simulate the controller models alongside the power electronic circuit of the inverter inside the real-time simulator.

A.1.2. ASGC CHIL

This controller hardware is the Austrian Institute of Technology Smart Grid Converter (ASGC) [4,18]. It supports a broad range of communication protocols including IEC61850, ModBus TCP, SunSpec, etc., to interact with external hardware. Moreover, it provides analog and digital wired interfaces to couple it with sensor outputs, PWM signals, and additional capabilities to couple it to the HIL-604 RTS, The controller is capable of full four-quadrant bidirectional operation and has various in-built functionalities such as Volt-VAR control, pf control, Volt-Watt control, low and high-voltage ride-through, etc.

A.1.3. Interface between HIL-604 and ASGC

The wired connection between HIL-604 and ASGC is based on a 192-pin on-board snap-in male-to-female configuration. This board makes all the 128 digital input and output pins available for easy access, and provides interfaces to couple with the analog channels as well.

A.2. Software utilization in details

The various software tools used in this research are outlined in this section.

A.2.1. Schematic editor

This software utilizes the Typhoon's component model library to construct the overall system model. While the library is smaller than those of other popular environments, it is possible to extend the library by incorporating user-defined models at the algorithmic level by using custom C functions or at the architectural level by assembling simpler blocks together [17].

A.2.2. HIL SCADA

This software provides a monitoring and control panel to interacts with the system model running on the real-time simulator. For the case of the ASGC, it also allows monitoring and adjustment of the controller. HIL SCADA provides data acquisition functions with capabilities to adjust the simulation model on run-time. It is possible to write macros that can help to automate simulation experiments, for example, applying a certain sequence of events. One such macro was developed for automating the GFOV testing. For the experiments reported below, two different implementations of the macro were developed to support the two different versions of HIL SCADA software that were used. HIL SCADA 8.4 (or above) was used for interacting with the model being simulated on HIL-604, while an older version – HIL SCADA 3.7 – was used for interacting with the ASGC controller.

A.2.3. aBoot Flasher

aBootFlasher is a software under MIT license provided by AIT. This is used to reconfigure the ASGC controller via USB COM port from the host PC. This reconfiguration can enable the ASGC controller to operate under different current and voltage ratings. This was an important requirement to analyze the SPOV functions of the controller.

A.2.4. Firmware manager

This tool manages the configuration of the HIL-604. Typhoon simulators can be configured to execute models using a number of parallel processor-cores. The configuration needs to be chosen judiciously and the model's schematic diagram must be carefully partitioned into those cores. This is required so that the model runs within the desired computation time per core and without over-runs. Presently Typhoon HIL-604 can operate in 5 different configurations, among which *Configuration 4* was found to suit the proposed experiments. This configuration partitions the simulator into three sizable processor cores that are large enough to house complex components such as inverters.

References

[1] Seppo Hänninen, Matti Lehtonen, Characteristics of earth faults in electrical distribution networks with high impedance earthing, Electr. Power Syst. Res. 44 (3) (1998) 155–161.

[2] Herbert B.-L. Lee, Sherret E. Chase, Roger C. Dugan, Overvoltage considerations for interconnecting dispersed generators with wye-grounded distribution feeders, IEEE Trans. Power Appar. Syst. PAS-103 (12) (1984) 3587–3594.

[3] Michael Ropp, Anderson Hoke, Sudipta Chakraborty, Dustin Schutz, Chris Mouw, Austin Nelson, Michael McCarty, Trudie Wang, Adam Sorenson, Ground fault overvoltage with inverter-interfaced distributed energy resources, IEEE Trans. Power Deliv. 32 (2) (2017) 890–899.

[4] Peter Jonke, Johannes Stöckl, Zoran Miletic, Roland Bründlinger, Christian Seitl, Filip Andrén, Georg Lauss, Thomas Strasser, Integrated rapid prototyping of distributed energy resources in a real-time validation environment, in: 2016 IEEE 25th International Symposium on Industrial Electronics (ISIE), 2016, pp. 714–719.

[5] P. Barker, Overvoltage considerations in applying distributed resources on power systems, in: IEEE Power Engineering Society Summer Meeting, Vol.1, 2002, pp. 109–114.

[6] Alberto Cerretti, Fabio Massimo Gatta, Alberto Geri, Stefano Lauria, Marco Maccioni, Giovanni Valtorta, Ground fault temporary overvoltages in MV networks: Evaluation and experimental tests, IEEE Trans. Power Deliv. 27 (3) (2012) 1592–1600.

[7] A. Cerretti, F.M. Gatta, A. Geri, S. Lauria, M. Maccioni, G. Valtorta, Temporary overvoltages due to ground faults in MV networks, in: 2009 IEEE Bucharest PowerTech, 2009, pp. 1–8.

[8] Janak R. Acharya, Yunfei Wang, Wilsun Xu, Temporary overvoltage and GPR characteristics of distribution feeders with multigrounded neutral, IEEE Trans. Power Deliv. 25 (2) (2010) 1036–1044.
[9] IEEE Guide for the Application of Neutral Grounding in Electrical Utility Systems, Part II–Synchronous Generator Systems, IEEE Std C62.92.2-2017 (Revision of IEEE Std C62.92.2-1989), 2017, pp. 1–38.
[10] Michael Ropp, Yinan Cui, Milad Kahrobaee, Dustin Schutz, Chris Mouw, On the sizing and benefits of grounding transformers with distribution-connected inverters, in: 2018 IEEE/PES Transmission and Distribution Conference and Exposition (T&D), 2018, pp. 1–5.
[11] Andy Hoke, Austin Nelson, Sudipta Chakraborty, Justin Chebahtah, Trudie Wang, Michael McCarty, Inverter ground fault overvoltage testing, 2015, 8.
[12] Alexandre B. Nassif, Eric Loi, Keaton A. Wheeler, Shay Bahramirad, Impact of IBR negative-sequence current injection on ground fault temporary overvoltage and ground overcurrent protection, in: 2022 IEEE/PES Transmission and Distribution Conference and Exposition (T&D), 2022, pp. 1–5.
[13] Jim Murphy, Huan Guo, Alternative 3V0 development for ground fault overvoltage protection with DERs/renewables interconnection (final report), 2021.
[14] Keaton A. Wheeler, Michael Simone, Alexandre B. Nassif, Yuji Takenobu, Tom Key, Wei Ren, Effective grounding criteria for high penetration inverter based resources in distribution networks, in: 2022 4th Global Power, Energy and Communication Conference (GPECOM), 2022, pp. 272–277.
[15] Gefei Kou, Kevin Phelps, Jonathan Deverick, Roland Brandis, Mark McVey, Ariel Valdez, Richard LaVigne, Aaron Reynolds, Mamadou Diong, Philip VanSant, Load rejection overvoltage of utility-scale distributed solar generation, IEEE Trans. Power Deliv. 35 (4) (2020) 2113–2116.
[16] Md Omar Faruque, T. Strasser, G. Lauss, V. Jalili-Marandi, Paul Forsyth, Christian Dufour, Real-time simulation technologies for power systems design, testing, and analysis, Power Energy Technol. Syst. J. IEEE 2 (2015) 63–73.
[17] Behrouz Azimian, Prottay M. Adhikari, Luigi Vanfretti, Hossein Hooshyar, Cross-platform comparison of standard power system components used in real time simulation, in: 2019 7th Workshop on Modeling and Simulation of Cyber-Physical Energy Systems (MSCPES), 2019, pp. 1–6.
[18] Blake Lundstrom, Sudipta Chakraborty, Georg Lauss, Roland Bründlinger, Russell Conklin, Evaluation of system-integrated smart grid devices using software- and hardware-in-the-loop, in: 2016 IEEE Power & Energy Society Innovative Smart Grid Technologies Conference (ISGT), 2016, pp. 1–5.
[19] Roland Bründlinger, Ron Ablinger, Zoran Miletic, AIT Smart Grid Converter(SGC) Controller featuring SunSpec protocol support utilizing Hardware-in-the-Loop (HIL) technology, 2016.
[20] Adrian Pan, Alexandru Bloi, Florin Molnar-Matei, From the balancing reactive compensator to the balancing capacitive compensator, Energies 11 (8) (2018).
[21] C. P. Sonia Rose, K. Suresh Kumar, K. Navin Kumar, Protection arrangements for grounded wye shunt capacitor bank, in: 2014 IEEE National Conference on Emerging Trends in New & Renewable Energy Sources and Energy Management (NCET NRES EM), 2014, pp. 63–69.
[22] A. Hoke, A. Nelson, B. Miller, S. Chakraborty, F. Bell, M. McCarty, Experimental Evaluation of PV Inverter Anti-Islanding with Grid Support Functions in Multi-Inverter Island Scenarios, Technical Report NREL/TP-5D00-66732, 2016.